Role of subband occupancy on electronic transport in quantum cascade detectors

A. Buffaz,[1] A. Gomez,[1,2] M. Carras,[2] L. Doyennette,[1] and V. Berger[1,2]
[1]*Laboratoire Matériaux et Phénomènes Quantiques, CNRS UMR 7162, Université Paris–Diderot, Bâtiment Condorcet, Case Courrier 7021, 75205 Paris Cedex 13, France*
[2]*Alcatel-Thales 3-5 lab, Route Départementale 128, 91767 Palaiseau Cedex, France*
(Received 6 October 2009; published 4 February 2010)

A model of the electronic transport in a quantum cascade structure under weak illumination in a very large temperature range is proposed. In a previous work, a simple model was shown to provide an expression of the quantum cascade detector (QCD) resistance in a range of temperature from 90 to 200 K. It relied on the assumption of the existence of a single, common quasi-Fermi level in a cascade of subbands, implying that the cascade is treated as a single reservoir of electrons. The electronic transport was successfully described with the doping density as the only adjustable parameter. However, it failed to reproduce experimental data at high temperatures. Indeed, in the latter range of temperatures (typically $T>200$ K) which is important for applications of QCDs, the transport inside a cascade of levels is governed by a specific resistance and a continuous potential distribution between subbands. A more sophisticated model including this local Fermi level description is developed in detail and compared to experimental data here. An excellent agreement is found between the calculated and measured resistance of the structure from 50 to 300 K, varying over typically eight orders of magnitude.

DOI: 10.1103/PhysRevB.81.075304 PACS number(s): 73.63.−b, 72.10.−d, 85.60.Bt, 85.60.Gz

I. INTRODUCTION

Quantum well infrared photodetectors (QWIPs) have become widely used quantum heterostructures for thermal imaging applications during the last 10 years. Major efforts have been devoted to improving their sensitivity, especially at detector temperatures above 80 K. Transport in such heterostructures, which involves both two-dimensional and three-dimensional electronic states in the quantum well and in the continuum, respectively, is a particularly difficult theoretical problem. Moreover, QWIPs are photoconductive detectors. The electric field—necessary to extract the electrons out of the wells—generates a dark current that results in a loss of sensitivity that can be detrimental to specific applications. For this reason, the quantum cascade detector (QCD) was initially proposed.[1–4] The electric field is replaced with a cascade of bound levels so that QCD works under no applied bias. Electrons only circulate between two-dimensional states. This makes the model of the electronic transport easier. Previous studies have indeed shown calculations of the electronic transport in QCDs without any adjustable parameter except the doping concentration.[5] Moreover, since the doped part is the first well, where the optical transition takes place, there are no space-charge effects and the Poisson equation is not required: the flat band condition is an excellent approximation. The device therefore represents a model system for the experimental study and theoretical modeling of electronic transport in such a complex multiple quantum well structure close to equilibrium.

The first model called "thermalized cascade model"[5]—describing the electronic transport in the absence of photons—calculates the resistance at zero bias times the detector area (R_0A) as a function of temperature over five orders of magnitude. However, some discrepancies between experiment and calculation are noticed at high ($T>200$ K) and low temperatures ($T<90$ K). This is a major problem for the development of QCDs for low background applications (low temperature, high performances) or, on the other hand, for high-temperature uncooled detection. There is a need for a model that allows the calculation of electronic transport in both ranges of temperature. This is the aim of this paper.

In Sec. II, the details of the typical QCD structure under study are presented and the principle of detection is recalled. The thermalized cascade model describing the electronic transport in the absence of photons is recalled in Sec. III and its limits highlighted in detail. Section IV is then devoted to a more sophisticated approach to transport in QCDs (the thermalized subbands model) that addresses both low and high temperatures. Finally, the R_0A can then be calculated and shown to fit the experimental data as a function of temperature over eight orders of magnitude between 40 K and room temperature. The thermalized subbands model consequently appears as an excellent theory for describing the resistance of a quantum cascade device close to equilibrium usefully applicable to optimization of the performance of these devices.

II. QCD STRUCTURE

The QCD under study is a GaAs/AlGaAs heterostructure designed to detect at a wavelength of 8 μm. It consists of ten periods of seven coupled QWs in GaAs and seven barriers in $Al_{0.34}Ga_{0.66}As$. The QWs (respectively, the barriers) have the following widths: 67.8, 19.8, 22.6, 28.3, 33.9, 39.6, and 45.2 Å (respectively, 56.5, 39.6, 31.1, 31.1, 31.1, 31.1, and 50.8 Å). The first QW of each period is *n* doped so that its first energy level E_G is occupied by electrons with a nominal Si doping concentration of 5×10^{11} cm^{-2}. The whole structure is embedded between two Si-doped GaAs contact layers. In Fig. 1 are presented the conduction band of one period and the modulus squared of the envelope function

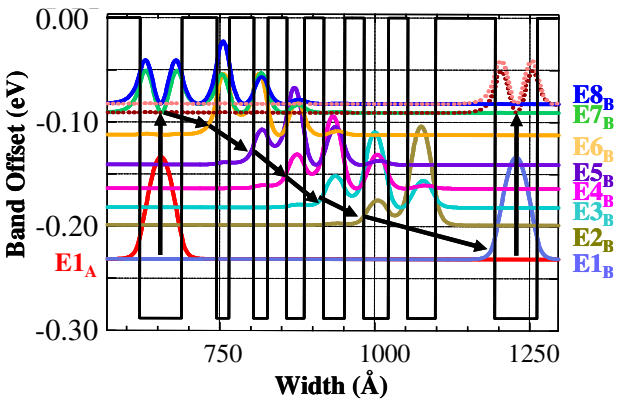

FIG. 1. (Color online) One period of an 8 μm QCD: conduction-band diagram, wave functions and associated energy levels. Black arrows recall the itinerary followed by an electron following to the absorption of a photon.

associated with each subband. The black arrows indicate the expected photoelectron path through the structure. Absorption of a photon induces an electron to jump from the ground state $E_{1,A}$ (mainly located in the first QW) to the two excited levels, $E_{7,B}$ and $E_{8,B}$ the wave functions of which are delocalized over the two first QWs. Large matrix elements between $E_{7,B/8,B}$ and lower energy levels ($E_{6,B}$ and $E_{5,B}$, in particular) allow the electron to be transferred to the right-hand QWs through longitudinal optical phonon relaxations and finally to the fundamental subband of the next period ($E_{1,B}$). This succession of subbands from $E_{8,B}$ to $E_{1,B}$ is hereafter designated as one cascade. Efficient electronic diffusion inside the cascade is necessary for the responsivity. The structure acts as a photovoltaic infrared detector and provides a detection signal at zero bias. The period is repeated N times in order to increase the detectivity. A complete experimental characterization of this detector was performed in Ref. 2 and gave the following results at 50 K: the resistivity at 0 V, R_0A, is equal to 3×10^5 Ω cm^2, the peak responsivity at 8 μm is 44 mA/W and the detectivity 4.5×10^{11} Jones. Thanks to these performances, it has been shown that this QCD detector is a very good candidate for thermal imaging applications, especially for long integration time conditions.

III. "THERMALIZED CASCADE" MODEL

A. Description

Contrary to a photoconductive QWIP, a QCD is designed to work in a photovoltaic way, i.e., under zero or close to zero applied bias. From an electronic point of view, a consequence is that the whole quantum structure is close to thermodynamical equilibrium. The dominant noise component in a QCD structure is a Johnson-type one,[6] usually expressed through the R_0A factor, the resistance at zero bias times the detector area. The case studied here is that of a device weakly illuminated so that the background noise is negligible as compared to the Johnson noise of the detector. In case of strong illumination, the photon noise should be taken into account.

We begin with a brief recall of the main results of the thermalized cascade model that was used in a previous study to evaluate the R_0A.[5] This will lead us to understand its limitations and particularly to bring to light the reasons why a new sophisticated approach is necessary.

The former model relies on two strong approximations. The first one consists in taking exclusively the electron-optical phonon (LO-phonon) interaction into account in the diffusion rate calculations. Indeed, the differences between energy levels of the QCDs are high enough to neglect the influence of the interaction between electrons and acoustical phonons.[7] Moreover, QCDs usually work around 80 K so elastic diffusion mechanisms such as interface roughness, alloy disorder, or impurity scattering can be neglected since they are only significant at very low temperature (4 K).[8] Finally, although electron-electron interaction is efficient for intrasubband diffusions, it is orders of magnitude lower than LO-phonon scattering for intersubband diffusion at our doping level.[9]

The global transition rate G_{ji} from a subband i of a cascade A to subband j of the neighboring cascade B is the sum of two components,

$$G_{ji} = G^e_{ji} + G^a_{ji}, \tag{1}$$

where the superscripts "a" and "e" stand, respectively, for absorption and emission of one LO phonon. Considering this approximation, G^e_{ji} can be expressed as

$$G^e_{ji}(0\ \text{V}) = \int_{E=E_j}^{\infty} dED(E)(n_{opt}+1)S^e_{ji}(E,E_j,E_i)f_j(E,E_{F_B}) \times[1-f_i(E-h\omega_{\text{LO}},E_{F_A})], \tag{2}$$

where E_i and E_j are the energies of the subbands i and j, E_{F_A} and E_{F_B} the quasi-Fermi levels of the cascades A and B, respectively. $D(E)$ is the density of states in a subband; it is constant and equal to $m^*/\pi\hbar^2$. f_i and f_j are subband i and j Fermi-Dirac occupation factors. n_{opt} is the Bose-Einstein statistics that accounts for phonon population. Finally, $S^e_{ji}(E,E_j,E_i)$ is the transition rate of an electron from an initial state of wave vector kj and energy E_j in the subband j toward the subband i; it is obtained through the integration of a matrix element involving a standard electron-optical-phonon Hamiltonian over all the possible final states of energy E_i in the subband i.

The second approximation of the thermalized cascade model lies in considering each cascade perfectly conductive. This results from a quantitative study of the transition rates in the structure. Indeed, intracascade rates ($G_{iB\text{-}jB}$) are several orders of magnitude larger than intercascade transition rates ($G_{jB\text{-}iA}$ and $G_{iA\text{-}jB}$) in the 90–150 K temperature range, as it has been shown in detail in Ref. 10. Each cascade is then considered as a reservoir of electrons at quasithermodynamical equilibrium characterized by a unique quasi-Fermi level, $E_{F_A}(E_{F_B})$ for the cascade A (B). This is similar to a p-n junction where the bias is applied between the two quasi-Fermi levels in the p and n zones, respectively. At thermodynamical equilibrium (V=0 V), the quasi-Fermi levels of consecutive cascades A and B are equal: no current circulates

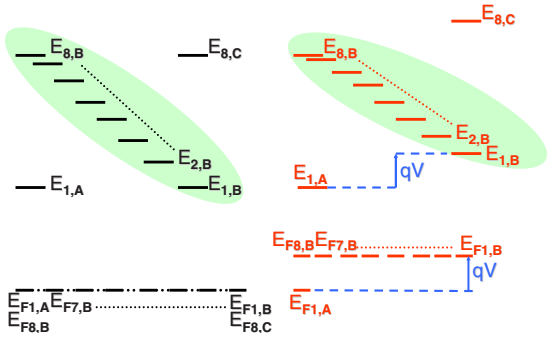

FIG. 2. (Color online) Schematic representation of thermalized cascade model. Left: thermodynamical equilibrium. Cascades A and B Fermi levels are equal, hence a null current in the structure. Right: positive bias. All quasi-Fermi levels of subbands of a cascade, $E_{F_j,B}$, for example, are equal; the bias is applied between E_{F_A} and E_{F_B}, the Fermi quasilevels of cascades A and B.

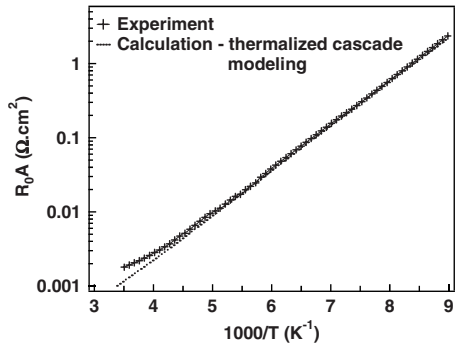

FIG. 3. Experimental and calculated R_0A as a function of the inverse of the temperature according to the thermalized cascade model. The doping concentration was set to 5×10^{11} cm^{-2} in the calculations.

in the structure. When a voltage is applied, all the bias is applied between the quasi-Fermi levels E_{F_A} and E_{F_B} as illustrated in Fig. 2.

The QCD resistance is governed by the transitions between consecutive cascades and the global density current is given by

$$J = q\sum_{i\in A}\sum_{j\in B}[G_{ji}(V) - G_{ij}(V)], \tag{3}$$

where G_{ij} (respectively, G_{ji}) corresponds to electronic transfers from a subband i of the cascade A to a subband j of the neighboring cascade B (respectively, from a subband j of the cascade B to a subband i of the neighboring cascade A) and q the electronic charge.

Analytical expressions for the QCD current density [Eq. (4)] around zero bias and for the R_0A parameter [Eq. (5)] (Ref. 5) can then be derived,

$$J = \frac{q^2V}{k_BT}\left[\sum_{i\in A}\sum_{j\in B}G_{ji}(0)\right], \tag{4}$$

$$R_0A = \frac{k_BT}{q^2\left[\sum_{i\in A}\sum_{j\in B}G_{ji}(0)\right]}. \tag{5}$$

In the above expression, k_B is the Boltzmann constant and T the temperature of the sample.

Both current and resistance can be expressed as a function of the transition rates $G_{ji}(0)$ calculated at equilibrium under zero voltage. The current can consequently be described as a sum of parallel channels, each one of them corresponding to an electron transfer G_{ji} from a subband j of the cascade B to a subband i of the neighboring cascade A.

Equation (5) has been used to estimate the resistance of the sample described in Sec. II. In Fig. 3 we compare the experimental and calculated R_0A as a function of the inverse of the temperature. The computed curve has been obtained using the doping concentration as an adjustable parameter. The best result was obtained with the value 5×10^{11} cm^{-2}. One can notice that this value happens to be the nominal doping concentration. An excellent agreement can be noticed between 90 and 200 K over five orders of magnitude in resistance. It is worth emphasizing that the electronic properties of such a complex quantum heterostructure are described without any other adjustable parameter.

B. Validity range of the model

As previously shown, the ≪thermalized cascade≫ model reproduces very satisfactorily the R_0A measurements from 90 to 200 K. However, outside this temperature range, discrepancies are visible (e.g., the relative error is 84% at 40 K and 32% at 280 K). This is a major issue. Indeed, shorter (3–5 μm) or longer (15 μm) wavelength detectors work at higher and lower temperatures, respectively. Moreover, 8 μm detectors are interesting at very low temperatures for low background thermal imaging and at high temperatures as uncooled detectors. It is also worth noticing that the minor discrepancies on the resistance calculation at high or low temperatures might be due to a poor understanding of the underlying physics. All these reasons point to the need for a transport model valid in a wider temperature range.

At low temperatures, the model fails to reproduce experimental curves because of the transition rate evaluations at exactly 0 V. Indeed, matrix elements are calculated between stationary-state solutions to the Schrödinger equation. But, at rigorously 0 V, several subbands belonging to distinct cascades are degenerate and wave functions are consequently strongly delocalized and coupled in the Schrödinger equation solution. This affects the matrix elements or the doping value used as an adjustable parameter. For the time being, in order to avoid these numerical difficulties, a low electric field is applied to the structure so that none of the levels are degenerate. It allows a correct evaluation of the transition rates in the structure, in accordance with the fact that coherent transport from one QCD period to another is not experimentally observed. Coherent transport within a period of a QCD is another topic that is currently under study.

Let us now focus on the high-temperature situation. The thermalized cascade model is based on the assumption of a very high electronic mobility inside a cascade of quantum levels; the corresponding calculated current flowing in the structure is overestimated at high temperature. A study of the

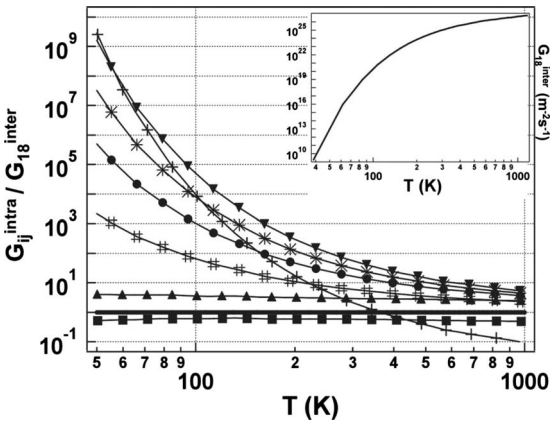

FIG. 4. Ratio between intracascade transition rates and intercascade transition rate as a function of temperature [+■: $G_{21}^{intra}/G_{18}^{inter}$; ▼: $G_{32}^{intra}/G_{18}^{inter}$; ●:$G_{43}^{intra}/G_{18}^{inter}$; *: $G_{54}^{intra}/G_{18}^{inter}$; #: $G_{65}^{intra}/G_{18}^{inter}$; ▲: $G_{76}^{intra}/G_{18}^{inter}$; and ■: $G_{86}^{intra}/G_{18}^{inter}$]. The inset gives the thermal evolution of G_{18}^{inter}.

responsivity under magnetic field has shown that intracascade transfers have similar amplitudes as intercascade ones at high temperatures.[10] This seems to indicate that intracascade rates are the limiting phenomenon at high temperature and therefore cannot be neglected. To confirm this hypothesis, the evolution of some of the intracascade transition rates (G_{ij} *with* $j=i-1$) as a function of the temperature has been compared to the main intercascade transition rate, G_{18}, related to the optical transition. The result is presented in Fig. 4 along with an inset giving G_{18} as a function of temperature. From 40 K up to 200 K, intracascade transition rates are found to be one or several orders of magnitude higher than the main intercascade one, justifying the approximation of quasithermodynamical equilibrium inside a cascade in this range of temperature. However, above 200 K, G_{18} (intercascade phenomenon) becomes very close to all the other intracascade transfer rates. As a result, cascades can no more be considered as being a reservoir at thermodynamical equilibrium and their contributions have to be considered in the overall resistance. The global hypothesis of a common quasi-Fermi level associated with each cascade has to be revisited and the field applied inside a cascade has to be taken into account in the current calculation. A more sophisticated model is consequently required.

In order to take into account the Fermi level drop inside the cascade, we shall now consider that a distinct quasi-Fermi level is associated with each subband of a cascade. This model we call "thermalized subbands" model. In this frame, one quasi-Fermi level $E_{F_{iB}}$ is related to each subband i of a cascade B. This assumption of intrasubband thermalisation is suitable since intrasubband relaxations [<100 fs (Ref. 11)] are much more efficient than the intersubband ones and, as a consequence, the electrons populate each subband according to a specific Fermi-Dirac distribution.

It is worth looking at Fig. 4 into more details since it provides very interesting information on the response mechanisms in a QCD and particularly on the cascade contribution to the photoresponse processes. One can note that whatever the temperature is, the intracascade transition rates G_{86} and

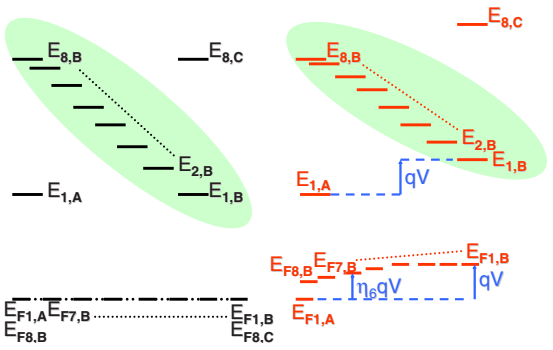

FIG. 5. (Color online) Schematic representation of thermalized subbands model. Left: thermodynamical equilibrium, subbands i and j (of cascades A and B) quasi-Fermi levels are aligned; there is no current in the structure. Right: under bias V. Each transition $E_{jB} \rightarrow E_{iA}$ absorbs a part $\eta_{ji}-1$ of the bias.

G_{76} responsible for extraction of photoexcited electrons are always of the same order of magnitude as G_{18}. This subject is beyond the scope of this paper and will be fully studied in a forthcoming publication but one can already assume that extraction probability of such a structure will be limited to roughly 50%. This is a drawback of the device since it directly affects the detector performance in terms of quantum efficiency. The design has thus to be modified to make extraction rates always higher than the relaxation probability rate to the ground state.

IV. THERMALIZED SUBBANDS MODEL

According to Sec. III, the QCD transport properties are not well described at high temperature ($T>200$ K) by the thermalized cascade model. Although [8–12 μm] wavelength detectors are generally supposed to operate around 80–90 K, increasing the working temperature could be interesting—at the cost of degrading performance—for applications. The detectors could then be candidates for Peltier-cooled room-temperature working conditions. This is the reason why a more sophisticated model that integrates intracascade transition rates is developed, enabling us to reproduce experimental R_0A curves outside the [90–200 K] temperature range.

The thermalized subbands approach is superior to the thermalized cascade model insofar as it regards not every cascade as being quasithermalized but each *subband within* a cascade. Differentiating each subband quasi-Fermi level introduces local resistivities; the cascade is thus made resistive, which we expect to be the reason for the global resistance increase at high temperature. The approximation is reasonable considering the extremely fast intrasubband thermalization. For instance, in the studied QCD, intrasubband lifetime is equal to a few hundred femtoseconds whereas intersubband lifetime is on the order of 1 ps. The hypothesis leads to associate its own Fermi quasilevel E_{F_j} to every subband E_{jB} of a cascade B.

At thermal equilibrium, all Fermi levels of the N consecutive cascades are aligned (see Fig. 5), i.e., $\forall j \in$ B, $\forall i \in$ A, and $E_{F_j}=E_{F_i}=E_F$. But when a bias V is applied, according to

thermalized subbands model, the Fermi quasilevels related to subbands within a cascade are not equal,

$$\forall j \in \mathrm{B}, \quad E'_{F_j} = E_F + \Delta E_{F_j} \text{ and } \forall i \in \mathrm{A},$$

$$E'_{F_i} = E_F + \Delta E_{F_i}, \tag{6}$$

$$E'_{F_{jB}} = E'_{F_{jA}} + qV. \tag{7}$$

In the current calculations, the electron-LO-phonon interaction is still the only one taken into account in the transition rate calculations. The approximation becomes even more accurate as temperature increases since other interactions (impurities and electron-electron scattering, interface roughness) hardly depend on the temperature whereas the electron-LO-phonon interaction increases.

A. Derivation of the current-density expression

The current is calculated by counting the number of electrons flowing through an imagined surface separating two consecutive cascades A and B. The global current density is given by the general equation

$$J = q\sum_{i\in A}\sum_{j\in B}[G_{ji}(V) - G_{ij}(V)]$$
$$= q\sum_{i\in A}\sum_{j\in B}[G^e_{ji}(V) - G^a_{ij}(V) + G^a_{ji}(V) - G^e_{ij}(V)]. \tag{8}$$

Within the context of thermalized subbands model, expressions of $G^e_{ji}(V)$ and $G^a_{ij}(V)$ involve the quasi-Fermi levels of the subbands $j(E_F+\Delta E_{F_j})$ and $i(E_F+\Delta E_{F_i})$,

$$G^e_{ji}(V) = \int_{E=E_j+\Delta E_j}^{\infty} dED(E)(n_{opt}+1)S^e_{ji} \times(E,E_j+\Delta E_j,E_i+\Delta E_i)f_j(E,E_F+\Delta E_{F_j}) \times[1-f_i(E-h\omega_{\mathrm{LO}},E_F+\Delta E_{F_i})], \tag{9}$$

$$G^a_{ij}(V) = \int_{E=E_j-h\omega_{\mathrm{LO}}+\Delta E_j}^{\infty} dED(E)n_{opt}S^a_{ij} \times(E,E_i+\Delta E_i,E_j+\Delta E_j)f_i(E,E_F+\Delta E_{F_i}) \times[1-f_j(E+h\omega_{\mathrm{LO}},E_F+\Delta E_{F_j})]. \tag{10}$$

The QCD current-density expression is derived in the same way as in the thermalized cascades model previously exposed; the only change lies in Fermi quasilevels that are now different for each of the N subbands j and i of cascades B and A.

Considering that transition rates are linked by the equality $S^a_{ij}(E+\hbar\omega_{\mathrm{LO}}+\Delta E_j,E_i+\Delta E_i,E_j+\Delta E_j) = S^e_{ji}(E+\Delta E_j,E_j+\Delta E_j,E_i+\Delta E_i)$, the difference $G^e_{ji}(V) - G^a_{ij}(V)$ can be rewritten as

$$G^e_{ji}(V) - G^a_{ij}(V) = \int_{E=E_j}^{\infty} S^e_{ji}(E+\Delta E_j,E_j+\Delta E_j,E_i+\Delta E_i)\alpha(E,V) \times[1-\gamma(E,V)]dE, \tag{11}$$

where

$$\alpha(E,V) = D(E)(n_{opt}+1)f_j(E+\Delta E_j,E_F+\Delta E_{F_B}) \times[1-f_i(E-h\omega_{\mathrm{LO}}+\Delta E_j,E_F+\Delta E_{F_A})] \tag{12}$$

and

$$\gamma(E,V) = \frac{n_{opt}f_i(E-h\omega_{\mathrm{LO}}+\Delta E_j,E_F+\Delta E_{F_A}) \times [1-f_j(E+\Delta E_j,E_F+\Delta E_{F_B})]}{(n_{opt}+1)f_j(E+\Delta E_j,E_F+\Delta E_{F_B}) \times [1-f_i(E-h\omega_{\mathrm{LO}}+\Delta E_j,E_F+\Delta E_{F_A})]}. \tag{13}$$

Since we are interested in the transport properties around 0 V, the product $\alpha(E,V)[1-\gamma(E,V)]$ can be expanded in series up to the first order with respect to the bias. This leads to the following expression:

$$\alpha(E,V)[1-\gamma(E,V)] = [\alpha^{(0)}+\alpha^{(1)}V+\vartheta(V)][1-\gamma^{(0)}+\gamma^{(1)}V+\vartheta(V)], \tag{14}$$

where $\alpha^{(i)}$ and $\gamma^{(i)}$ are the ith term of the series expansion as a function of the bias and $\lim_{V\to 0}\vartheta(V)/V=0$.

Given Eqs. (12) and (13), we find

$$\alpha^{(0)} = \alpha(E,0) = D(E)(n_{opt}+1)f_j(E,E_F) \times[1-f_i(E-h\omega_{\mathrm{LO}},E_F)] \text{ and } 1-\gamma^{(0)} = 1-\gamma(E,0) = 0. \tag{15}$$

Introducing the expressions of Fermi-Dirac and Bose-Einstein statistics and linearizing the result around 0 V, we obtain

$$\gamma^{(1)} = \frac{q}{k_BT}. \tag{16}$$

It is here worth noticing that this result does not depend on variations in the subband positions ΔE_j. Taking into account

expressions (13)–(15), the difference $G^e_{ji}(V)-G^a_{ij}(V)$ then becomes

$$G^e_{ji}(V) - G^a_{ij}(V) = \frac{1}{k_B T} \cdot \Delta E_{F_{ji}} \cdot G^e_{ji}(0), \tag{17}$$

where $\Delta E_{F_{ji}}=\Delta E_{F_j}-\Delta E_{F_i}$. Likewise, the term $G^a_{ji}(V)-G^e_{ij}(V)$ can be expressed as

$$G^a_{ji}(V) - G^e_{ij}(V) = \frac{1}{k_B T} \cdot \Delta E_{F_{ji}} \cdot G^a_{ji}(0). \tag{18}$$

This leads finally to the expression

$$G_{ji}(V) - G_{ij}(V) = \frac{1}{k_B T} \cdot \Delta E_{F_{ji}} \cdot G_{ji}(0). \tag{19}$$

The bias can no longer be assumed to be absorbed between quasilevels of two neighboring cascades (i.e., $\forall j \in \mathrm{B}$, $\forall i \in \mathrm{A}$, and $\Delta E_{F_{ji}}=qV$) but intracascade resistances—represented by the N quasi-Fermi levels of the N subbands of a cascade—have to be taken into account. We define η_i as $\Delta E_{F_{j,B}}=\eta_j qV$ and η_{ji} as $\eta_{ji}=\eta_j-\eta_i$. Therefore, the term $(1+\eta_{ji})$ accounts for the proportion of bias between subbands i and j of two consecutive cascades A and B as described in Fig. 5,

$$\Delta E_{F_{ji}} = \Delta E_{F_{j,B}} - \Delta E_{F_{i,A}} = \eta_j qV - (\eta_i - 1)qV = qV(\eta_{ji} + 1). \tag{20}$$

Equation (17) can now be rewritten as

$$G_{ji}(V) - G_{ij}(V) = \frac{qV}{k_B T}(\eta_{ji} + 1) \times G_{ji}(0). \tag{21}$$

In this new approach, the bias is distributed gradually along the cascade, clearly represented in Fig. 5. One can also note that the case of thermalized cascade model corresponds to all $\eta_j=1$, i.e., $\forall(i,j)$, $\eta_{ij}=0$, and $\Delta E_{F_{ji}}=qV$.

The current density flowing through the QCD structure can now be expressed as

$$J = \frac{q^2 V}{k_B T} \sum_{i \in A} \sum_{j \in B} (\eta_{ji} + 1) \times G_{ji}(0). \tag{22}$$

Consequently, the figure of merit R_0A becomes

$$R_0 A = \frac{k_B T}{q^2 \sum_{i \in A} \sum_{j \in B} (\eta_{ji} + 1) \times G_{ji}(0)}. \tag{23}$$

Contrary to the previous thermalized cascade model, this approach requires solving a homogeneous rate equation system involving all of the possible transfer rates in the QCD structure (intercascade and intracascade ones). This is necessary to calculate the η_{ij} factor in expression (23). Let us remark that for significant $G_{ji}(0)$, i is low ($i=1$ or 2 typically) and j is high ($j=6$, 7, or 8) and $\eta_{ji}<0$.

B. Calculation of η_{ij}

To write the rate equation, let us consider a system made of three consecutive cascades A, B, and C. We focus on a subband j of the central cascade B. For each subband, the stationary state is expressed as follows:

$$\forall j \in \mathrm{B}, \quad \sum_{i \in A} [G_{ji}(V) - G_{ij}(V)] + \sum_{i \in B, i \neq j} [G_{ji}(V) - G_{ij}(V)] + \sum_{i \in C} [G_{ji}(V) - G_{ij}(V)] = 0. \tag{24}$$

Inserting Eq. (21) into Eq. (24) allows us to reformulate the rate equation as a function of transition rates at equilibrium,

$$\forall j \in \mathrm{B}, \quad \sum_{i \in A} G_{ji}(0)(\eta_{ji} + 1) + \sum_{i \in B, i \neq j} G_{ji}(0)\eta_{ji} + \sum_{i \in C} G_{ji}(0)(\eta_{ji} - 1) = 0. \tag{25}$$

Transition rates will from now on be indexed by AB and CB superscripts for intercascade transitions, and by BB for intracascade ones,

$$\forall j \in \mathrm{B}, \quad \sum_{i=1}^{N} G^{AB}_{ji}(0)(\eta_{ji} + 1) + \sum_{i=1, i \neq j}^{N} G^{BB}_{ji}(0)\eta_{ji} + \sum_{i=1}^{N} G^{CB}_{ji}(0)(\eta_{ji} - 1) = 0. \tag{26}$$

Because of periodicity, $G^{AB}_{ji}=G^{CB}_{ji}$, leading to the following expression:

$$\forall j \in \mathrm{B}, \quad \sum_{i=1}^{N} G^{AB}_{ji}(0)(\eta_{ji} + 1) + \sum_{i=1, i \neq j}^{N} G^{BB}_{ji}(0)\eta_{ji} + \sum_{i=1}^{N} G^{BA}_{ji}(0)(\eta_{ji} - 1) = 0. \tag{27}$$

Assuming $G^{BB}_{jj}(0)=0$, this can be rewritten as

$$\forall j \in \mathrm{B}, \quad \sum_{i=1}^{N} [G^{AB}_{ji}(0) + G^{BB}_{ji}(0) + G^{BA}_{ji}(0)]\eta_i - \sum_{i=1}^{N} [G^{AB}_{ji}(0) + G^{BB}_{ji}(0) + G^{BA}_{ji}(0)]\eta_j = \sum_{i=1}^{N} [G^{AB}_{ji}(0) - G^{BA}_{ji}(0)]. \tag{28}$$

This leads to the following matrix system, the terms of which will be detailed hereafter:

$$M \cdot H = \Delta G. \tag{29}$$

H is a vector of dimension N related to the N Fermi quasilevels η_j of the different subbands of a cascade,

$$H = \begin{pmatrix} \eta_1 \\ \eta_2 \\ \vdots \\ \eta_N \end{pmatrix}.$$

M is an N*N matrix with elements,

$$M_{ji} = (G_{ji}^{AB} + G_{ji}^{BB} + G_{ji}^{BA}) - \delta_{ji}\sum_{k=1}^{N}[G_{jk}^{AB} + G_{jk}^{BB} + G_{jk}^{BA}]. \tag{30}$$

Finally, ΔG is a vector of dimension N; its components are

$$\Delta G_j = \sum_{i=1}^{N}(G_{ji}^{AB} - G_{ji}^{BA}). \tag{31}$$

Since all G_{ij} are calculated at 0 V, the sum $\Sigma_{j=1}^{N}\Delta G_j$ is equal to zero; thus, Eq. (29) results in a system of $N-1$ independent equations with N unknowns. Setting $\eta_1=1$ as reference yields the Nth equation.

C. Physical meaning of η_j: Diode nonideality

In a classical diode, the current is expressed as $J=J_{sat}[\exp(\frac{qV}{k_BT})-1]$. This expression has to be compared to that of the QCD, i.e.—considering only the major transition for the sake of simplicity $J_{\mathrm{QCD}}=J_{sat}[\exp(\frac{\eta_8 qV}{k_BT})-1]$. This clearly brings into light the physical meaning of the term η_j, which expresses the diode nonideality. Figure 5 provides another way of illustrating the signification of η_j.

According to thermalized cascade model, an electron incident on a level $j(j\neq 1)$ of the period B goes instantaneously into the ground state of the next period because the cascade by assumption provides no resistance against the electron circulation. It can consequently be considered that no bias is applied to it: a unique Fermi level is associated to the whole cascade and all the voltage is applied between the Fermi levels of cascades A and B. In a way, as previously remarked, $\eta_j=1\,\forall\, j$.

In the thermalized subbands approach, cascade resistances are taken into account through the N quasi-Fermi levels associated with the N subbands of a cascade. Because of periodicity, each Fermi quasilevel $E_{F_j}=E_F+\Delta E_{F_j}$ of the cascade B is moved by an amount qV compared with the equivalent subband j of the cascade A. In other words, $E_{F_{j,B}}=E_F+\eta_j qV$ and $E_{F_{j,A}}=E_F+(\eta_j-1)qV$.

The thermalized subbands model enables making allowance for the voltage drop along the cascade. As far as level 1 is concerned, $\eta_1=1$ and $E_{F_{1,B}}-E_{F_{1,A}}=qV$. But when j increases, η_j becomes less than 1, which means that $E_{F_{j,B}}-E_{F_{1,A}}=\eta_j qV<qV$. A series of bias repartition can be noticed in the cascade B. η_j values are given in Table I at several detector temperatures and plotted on Fig. 6 in which two regimes can be distinguished.

From 100 to 200 K, values of η_j, $j\in[2,6]$ are quite stable and close to 1. This means that transfers via these subbands are efficient, and the bias applied between the levels jB and the ground state iA is almost qV. The situation is different for the levels $E_{7/8B}$. For example, $\eta_7\approx 0.85$, which shows that electronic transfer from this subband is more difficult. This is due to the small overlap between this level and the other subbands in the cascade. It is even worse for level 8 for which the value of η_8 falls between 0.3 and 0.4. This will have some impact on the detector quantum efficiency and will be discussed in a forthcoming publication devoted to the detector performances.

TABLE I. η_j as a function of temperature.

η_j	100 K	125 K	165 K	193 K	232 K	305 K	386 K
$j=2$	1	1	0.98	0.96	0.89	0.7	0.5
$j=3$	1	1	0.98	0.96	0.89	0.69	0.5
$j=4$	1	1	0.98	0.95	0.89	0.69	0.49
$j=5$	1	1	0.98	0.94	0.87	0.66	0.47
$j=6$	0.98	0.97	0.95	0.9	0.83	0.62	0.43
$j=7$	0.84	0.85	0.84	0.8	0.74	0.56	0.38
$j=8$	0.28	0.33	0.37	0.39	0.38	0.3	0.22

The second regime is observed above 200 K where all the η_j decrease when temperature rises. This reflects a reduction in the intracascade transfer efficiency relative to intercascade ones. This translates into a nonideality of the diode in the expression for its current.

D. Calculation of the R_0A parameter

The QCD resistance under no bias in the thermalized subbands approach is given by Eq. (23). In the case of the thermalized cascade model $\forall j$, $\eta_j=1$, therefore, $\eta_{ji}=\eta_j-\eta_i=0$; the previous formula is reduced to expression (5).

It may be worth noticing that, from a device point of view, serial resistances are always detrimental for the detectivity and therefore intracascade resistance should be avoided. Since dark current in QCD is mainly controlled by transitions between the cascade A ground state E_{1A} and the different levels j of the following period B, R_0A can be approximated by

$$R_0A = \frac{k_BT}{q^2\sum_{j=1}^{N}\eta_j\times G_{j1}(0)}. \tag{32}$$

Through this formula, QCD current appears as a sum of currents $[\frac{q^2}{k_BT}G_{j1}\Delta E_{F_{j1}}]$ in parallel, each level j representing a channel likely to be followed by the current toward E_{1A}.

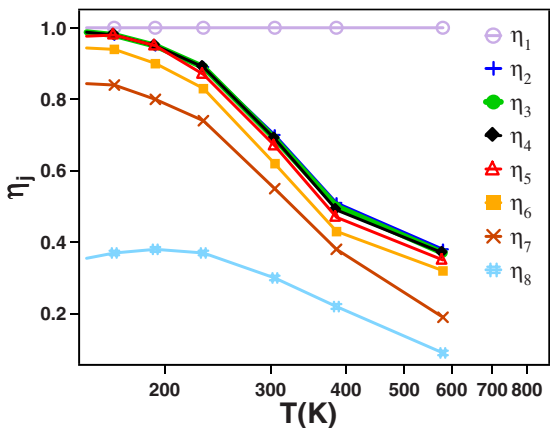

FIG. 6. (Color online) η_j as a function of temperature.

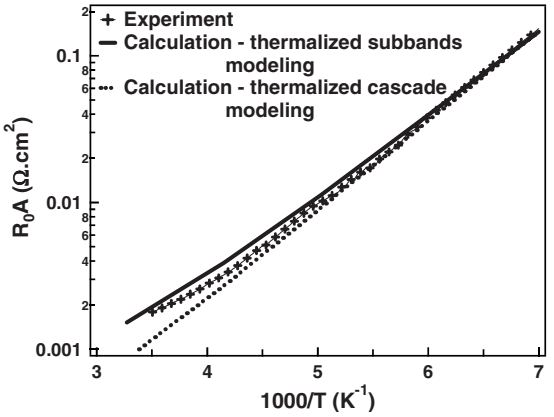

FIG. 7. Experiment and the two calculated R_0A—in the thermalized cascade and thermalized subbands approaches—as a function of the inverse of the temperature between 100 and 300 K. It highlights the "thermalized subbands model" ability to reproduce the R_0A increase above 200 K (which the previous model failed to do).

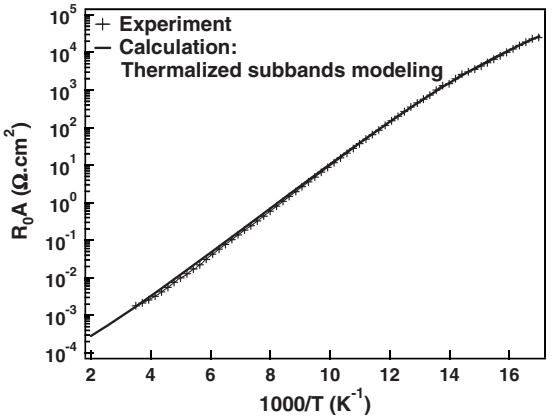

FIG. 8. R_0A calculation in accordance with Eq. (32) and the thermalized subbands model. (for 500 V/cm electric field and a doping level equal to 3.5×10^{11} cm^{-2}). A fine agreement over eight orders of magnitude can be remarked between experiment and calculation from 40 to 300 K.

Because of the series resistors present in the cascade, the bias applied to every channel j is not qV but rather $\eta_j qV$. Therefore, when summing all the currents, $G_{j1}(0)$ decreases by a η_j factor. This accounts for the R_0A increase with the temperature. Indeed, at high temperatures, electronic transport is dominated by the transitions $E_{7/8B}\rightarrow E_{1A}$, a rise in temperature causes the cascade resistivity to increase, which results in a decrease in η_7 and η_8 (see Table I and Fig. 6). This corresponds to a smaller bias applied between Fermi levels of the subbands responsible for the current flowing in the structure. The emergence of these local resistances in the cascade explains the global resistance increase at high temperature.

Expression (32) has been used to calculate the ten period-QCD resistance at 0 V in a wide temperature range with a doping density equal to 3.5×10^{11} cm^{-2}. Figure 7 presents the result for the high temperatures along with the experimental R_0A and the result of the thermalized cascade model. It clearly shows that the thermalized subbands approach fits experimental measurements much better than the thermalized cascade model in this temperature range. Figure 8 finally shows that the thermalized subbands approach makes it possible to reproduce the experimental 0 V resistance with an excellent accuracy over eight orders of magnitude.

V. CONCLUSION

A model including different Fermi levels in each subband of a cascade has been developed. The different quasi-Fermi levels are determined by solving a complete set of rate equations, based on the transfer rates of electrons from subband to subband through the electron-phonon interaction. This new approach allows taking into account the resistance of a cascade of levels which is all the more important since the intracascade resistance acquires a significant role in comparison to the intercascade resistance in the case of high temperatures, typically greater than 200 K. This model has finally been confronted with experimental data and an excellent agreement has been found over eight orders of magnitude of variation in the resistance, i.e., for temperatures varying from 40 K to room temperature.

[1] L. Gendron, M. Carras, A. Huynh, V. Ortiz, C. Koeniguer, and V. Berger, Appl. Phys. Lett. **85**, 2824 (2004).
[2] L. Gendron, C. Koeniguer, and V. Berger, Appl. Phys. Lett. **86**, 121116 (2005).
[3] M. Graf, G. Scalari, D. Hofstetter, J. Faist, H. Beere, E. Linfield, D. Ritchie, and G. Davies, Appl. Phys. Lett. **84**, 475 (2004).
[4] G. Scalari, M. Graf, D. Hofstetter, J. Faist, H. Beere, and D. Ritchie, Semicond. Sci. Technol. **21**, 1743 (2006).
[5] C. Koeniguer, G. Dubois, A. Gomez, and V. Berger, Phys. Rev. B **74**, 235325 (2006).
[6] A. Gomez, M. Carras, A. Nedelcu, E. Costard, X. Marcadet, and V. Berger, Proc. SPIE **6900**, 69000J (2008).
[7] J. Radovanovic, V. Milanovic, Z. Ikonic, D. Indjin, and P. Harrisson, J. Appl. Phys. **97**, 103109 (2005).
[8] A. Leuliet, A. Vasanelli, A. Wade, G. Fedorov, D. Smirnov, G. Bastard, and C. Sirtori, Phys. Rev. B **73**, 085311 (2006).
[9] S. M. Goodnick and P. Lugli, Phys. Rev. B **37**, 2578 (1988).
[10] A. Gomez, N. Péré-Laperne, L.-A. de Vaulchier, C. Koeniguer, A. Vasanelli, A. Nedelcu, X. Marcadet, Y. Guldner, and V. Berger, Phys. Rev. B **77**, 085307 (2008).
[11] The intrasubband relaxation time, τ_2, is given by the full width at half maximum related to the spectral response (1 μm in the studied QCD).